UNIVERSITY OF LEEDS

This is a repository copy of *Modelling of multi-minerals kinetic evolution in hyper-alkaline leachate for a 15-year experiment*.

White Rose Research Online URL for this paper:
https://eprints.whiterose.ac.uk/162890/

Version: Accepted Version

eprints@whiterose.ac.uk
https://eprints.whiterose.ac.uk/

Modelling of multi-minerals kinetic evolution in hyper-alkaline leachate for a 15-year experiment

Yousef Baqer[1], XiaoHui Chen[1]*, Christopher Rochelle[2], Steven Thornton[3]

School of Civil Engineering, University of Leeds, LS2 9JT

[1]*School of Civil Engineering, University of Leeds.

Telephone: +44 (0)113 3430350

Email: x.chen@leeds.ac.uk

[2] British Geological Survey

[3] Groundwater Protection and Restoration Group, Dept of Civil and Structural Engineering, The University of Sheffield

18   *Abstract*

19

20   Cement has been widely used for low- to intermediate-level radioactive waste management;

21   however, the long-term modelling of multiple mineral transfer between the cement leachate and

22   the host rock of a geological disposal facility remains a challenge due to the strong physical-

23   chemical interactions within the chemically-disturbed zone. This paper presents a modelling study

24   for a 15-year experiment simulating the reaction of crystalline basement rock with evolved near-

25   field groundwater (pH = 10.8). A mixed kinetic equilibrium (MKE) modelling approach was

26   employed to study the dolomite-rich fracture-filling assemblage reacting with intermediate cement

27   leachate. The study found that the mineralogical and geochemical transformation of the system

28   was driven by the kinetically-controlled dissolution of the primary minerals (dolomite, calcite,

29   quartz, k-feldspar and muscovite). The initial high concentration of calcium ions appeared to be

30   the main driving force initiating the dedolomitization process, which played a significant role in

31   the precipitation of secondary talc, brucite and Mg-aluminosilicate minerals. The modelling study

32   also showed that most of the initially precipitated calcium silicon hydrate phases redissolved and

33   formed more stable calcium silicon aluminium hydrate phases. The findings highlight the

34   importance of a deep and insightful understanding of the geochemical transformations based on

35   the type and characteristics of the host rock, where the system is under out of equilibrium

36   conditions, and the rates of mineral reactions.

37

40

1. Introduction

Underground geological facilities are the most secure places to store/dispose of radioactive wastes generated during the civil/military programmes, and also generated through scientific, engineering and medical usage. One concept for low- and intermediate-level radioactive waste involves constructing an underground facility in a host rock at a depth of several hundred metres, then backfilling with a cementitious material. Such a facility is designed to achieve two main safety objectives: 1) to isolate the radioactive waste from the biosphere, and 2) to provide multiple barriers (including a high pH environment) to minimise radionuclide mobility over long timescales.

The containment system involves multiple barriers in which the engineered barriers work alongside natural ones (e.g. stable and low permeability host rock) to prevent the release of radionuclides to the biosphere. The concept has been adopted by several countries, including the UK, Sweden and South Korea (Authority 2010a; Francis et al. 1997; Kim et al. 2007; Skogsberg and Ingvarsson 2006). The final design and performance assessment of the engineered barrier can be influenced by the waste inventory, the surrounding conditions that can be expected during the performance assessment timescale and the degree of reaction with the surrounding host geology. Usually, the near field plays a crucial role in providing long-term control over radionuclide migration, which limits their release to the surrounding environment. Over time, the chemical properties (e.g., sorption capacity, reactive surface area) and physical properties (e.g., porosity, permeability) of the host rock in the near field barrier evolve as a result of the interactions with their surroundings and with other barriers. As this will happen long before any potential migration

64 of radionuclides, it is useful to understand and to be able to predict these changes, as they are likely

65 to influence potential radionuclide retardation.

66

67 One of the challenges in evaluating the effectiveness of an engineered barrier is understanding the

68 extent to which the evolving process of the near field host rock may occur. This will help in

69 assuring that the engineered barrier materials will fulfil their safety functions over performance

70 assessment timescales. The evolution of near field properties will strongly be linked to the

71 interaction of the host rock and high pH water leaching out of the cement (the 'alkaline disturbed

72 zone', ADZ).

73

74 Cement leachate is usually formed when the facility is closed and becomes saturated with

75 groundwater that then reacts and equilibrates with the cementitious engineered barrier. The

76 reaction process results in a high-pH plume that inhibits corrosion and limits some radionuclide

77 solubility. Eventually, some cement leachate will migrate into the surrounding rock and create a

78 chemically disturbed zone (CDZ) at the interface between the cement barrier and the host rock,

79 initiating a series of reactions (Chen et al. 2016; Chen and Thornton 2018; Chen et al. 2015). The

80 dissolution of primary minerals in the host rock is likely to be accompanied by precipitation of

81 new minerals with evolved chemical and physical properties that may contribute to decreased

82 radionuclide mobility through processes such as the reduction in permeability, increased sorption,

83 and coprecipitation.

84

85 For a cement-based geological disposal facility, several experimental studies and numerical

86 models have been performed to demonstrate the reaction of highly-alkaline cement leachate with

87   minerals in the host rock (Berner 1990; Harris et al. 2001a; Harris et al. 2001b; Schwyn et al.

88   2003). Previous research has considered three cement leachate evolution stages based on the

89   progression of pH values (Small et al. 2016), which can be summarised as: young cement leachate

90   (YCL), intermediate cement leachate (ICL) and old cement leachate (OCL). The reaction of ICL

91   with the near field host rock is the focus of this study, and this may result in the formation of a

92   changing series of mineral assemblages, changes to mineral surfaces, variations in pH, as well as

93   other changes (Moyce et al. 2014). These processes will eventually affect the sorption capability

94   of radionuclides at the mineral surface (Authority 2010b).

95

96   The paper models mineral evolution in a 15-year laboratory experiment, analysing interlinks

97   among multiple minerals known to occur in Borrowdale Volcanic Group (BVG) rocks in reaction

98   with ICL (the BVG is an important basement rock in north-west England, and which was

99   previously investigated by UK Nirex Limited (Francis et al. 1997). Importantly, the rock sample

100   comprised a hydraulically-conductive dolomite-rich fracture, and thought dolomite is only a minor

101   phase in the rock overall; it is a major phase in direct contact with current groundwater. The

102   modelling process implements the concept of a mixed kinetic equilibrium approach (MKE), which

103   combines the advantages of both equilibrium and kinetic formulations to enable the modelling of

104   complex geochemical reactions (Bethke 1994; Bethke 1996; Chen and Thornton 2018; Van der

105   Lee 1997; Van der Lee 1998; Westall 1986). This approach was initially developed to overcome

106   the shortage of kinetic data for minerals that dissolve and precipitate (Soetaert et al. 1996),

107   assuming a faster reaction by means of the equilibrium concept and a slower reaction controlled

108   by the kinetic process (Atkinson et al. 1988; Hoch et al. 2012). The model is used to develop a

109 deeper understanding of the pH evolution along with quantification of the amount of host rock

110 minerals dissolving or precipitating in the near field/alkaline disturbed zone.

111

112 *2. Experimental study*

113

114 The experiment was conducted by the British Geological Survey (Moyce et al. 2014; Rochelle et

115 al. 2016; Rochelle et al. 1997) over the course of 15 years, starting in 1995, and being part of a

116 larger series of experiments of different durations. The original intent of the experiment was to

117 study the reaction of a sample of Ordovician age Borrowdale Volcanic Group (BVG) rock with

118 both a pH 13 'young near-field porewater' (YNFP) and a pH 12 'evolved near-field groundwater'

119 (ENFG) (rock type and fluid naming convention based on that used in the Nirex Safety Assessment

120 research programme [NSARP] at the time). These fluids represent, respectively, 'young cement

121 leachate (YCL) and 'intermediate cement leachate' (ICL) (naming convention used in the

122 BIGRAD project) released from a representative cementitious barrier that could be used in a deep

123 geological disposal facility for intermediate-level radioactive waste. Although the experiments

124 significantly exceeded their originally planned durations and also that of the NSARP, it was useful

125 to continue them as the BVG contains many mineral phases typical of crystalline basement rocks

126 in general. In the experiment of relevance to the study presented here, a dolomite-rich fracture

127 assemblage in the BVG was reacted with YNFP, and the resultant solid and fluid products initially

128 examined after 15 months and also for up to 15 years. The focus of the current study was to better

129 understand the mineralogical evolution of this experimental system for the entire 15 years, in order

130 to investigate longer-term geochemical processes.

131
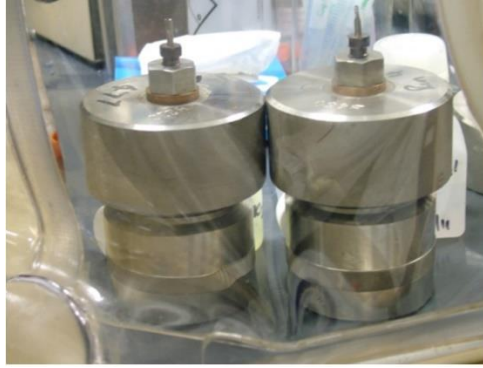
133   Figure 1: Stainless steel pressure vessels lined with Teflon® used to contain the BVG and synthetic CDZ-type fluid
134   experiments.

135

136   Two PTFE-lined stainless steel vessels, of 150 mL and 100 mL, were used for the 'reacting' and

137   blank experiments, respectively (Figure 1). The solid phase consisted of a piece of drill core

138   containing altered wall rock and a dolomite-rich fracture fill from a hydrogeological conductive

139   fracture zone in the BVG. The 2-kg rock sample was then disaggregated and sieved (Moyce et al.

140   2014; Rochelle et al. 1997). In the 'reacting' experiment, 35 g of disaggregated BVG was used

141   with 140 g of groundwater-cement leachate, and the stainless-steel vessel was kept in a 70°C oven.

142   The smaller blank experiment just contained the leachate. The ENFG leachate was presented by

143   slightly saline water (Na/CaCl) saturated with $Ca(OH)_2$ (Table 1). All preparation processes were

144   performed under a nitrogen atmosphere to prevent reaction of the alkaline water with atmospheric

145   carbon dioxide. During the reaction, the rock underwent mineralogical changes that changed the

146   concentration of the dissolved ions in the ENFG leachate. Experiments were terminated and

147   sampled after the fourth, ninth and fifteenth months (Rochelle et al. 2016; Rochelle et al. 1997),

148   and importantly also at the end of the fifteenth year (Moyce et al. 2014). The solid experimental

149   residues were washed in propan-2-ol and then dried prior to storage and analysis. For X-ray

150   diffraction analysis, a subsample was milled and a 10% corundum (Al_2O_3) standard added. A

151   diffractometer instrument (PANalytical X'Pert Pro) with PANalytical X'Pert Highscore Plus

152   software was then used to carry out the final mineralogical analysis (Moyce et al. 2014; Rochelle

153   et al. 2016).

154

155 Table 1: Composition of the Evolved Near-Field Groundwater (ENFG) prepared by the British Geological Survey
156 (Rochelle et al. 2016; Rochelle et al. 1997).

| Chemical component	Concentration (mg/L)
Al	4.17
B	0.335
Ba	0.017
Br	23.2
CO_3	20
Ca	1930
Cl	15100
F	0.03
Fe	0.120
K	185
Li	0.153
Mg	0.117
Mn	0.010
Na	9160
SO_4	1090
NO_3	20
Si	2.07
Sr	166
pH (at 70ºC)	10.84

157

158 ## 3. Modelling methodology

159

160   The conceptual model developed for this study is presented in Figure 2. The idea was developed

161   based on theoretical and experimental analysis. The MKE approach is based upon the timescale of

162   each mineral reaction rate (i.e., which reaction is faster and which slower). For each mineral, either

163   a kinetic or equilibrium approach, or a mix of both (if the difference between rates was more than

164   10^2), was used to provide the supporting information for the software. The concept of MKE has

165   been widely implemented in subsurface geochemical applications, as it allows both kinetic and

166 equilibrium reactions to model a multiphase and multi-component system (Brun and Engesgaard

167 2002; Lichtner 1996; Mayer et al. 2002; Prommer et al. 2003).

168
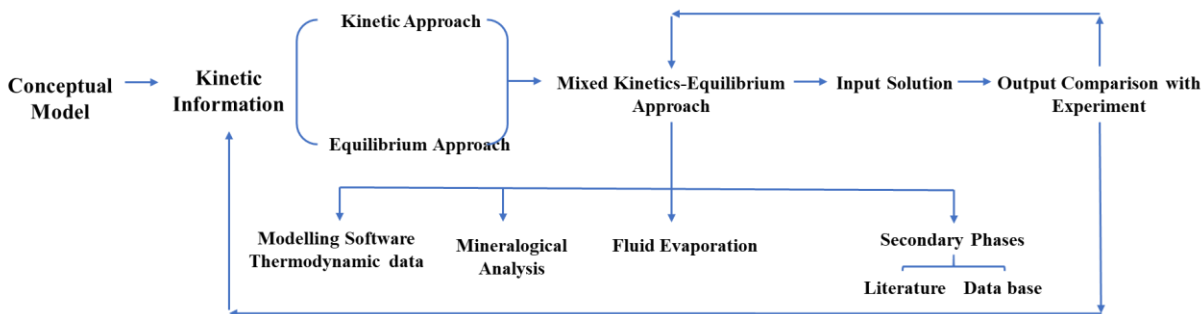
169

171

172 ### 3.1. Conceptual model software and thermodynamic data

173 The simulation carried out in this study was performed with the PHREEQC code (version 3.6.1).

174 The software can compute a wide range of chemical reactions in aqueous geochemical systems,

175 utilising both chemical thermodynamic and kinetic data. In recent years, several databases have

176 been developed by various authors to optimise the use of this geochemical code. For a cement

177 leachate–host rock reaction in an underground repository, the Lawrence Livermore National

178 Laboratory (LLNL), Thermoddem, Thermoddem DB and CEMDATA DB databases were applied

179 by previous researchers (Blanc et al. 2012; Lothenbach et al. 2019; Wolery 1992; Wolery and

180 Daveler 1992). In this work, LLNL database (Delany and Lundeen 1990) –was utilise though with

181 some modifications, namely; the addition of kinetic information for calcium silicon hydrate (CSH)

182 and calcium silicon aluminium hydrate phases (CASH). This database seemed to be the best option

183 available since it has kinetic information for a variety of minerals and aqueous species, especially

184 carbonate minerals that are required for the simulation of phases present in the BVG rock sample.

185 The data of thermodynamic reactions (equilibrium constants) for the major minerals are shown in

186   Table 2 (Chen and Thornton 2018). Note that the below values of $log\,K_{eq}$ are valid for the

187   experiment condition.

188

189   Table 2: Reactions and equilibrium constants for minerals used in the calculations.

Mineral	Reaction	Log Keq
Calcite	$CaCO_3 + H^+ = Ca^{++} + HCO_3^-$	1.8487
Muscovite	$KAl_3Si_3O_{10}(OH)_2 + 10H^+ = K^+ + 3Al^{+++} + 3SiO_2 + 6H_2O$	13.5858
Kaolinite	$Al_2Si_2O_5(OH)_4 + 6H^+ = +2Al^{+++} + 2SiO_2 + 5H_2O$	6.8101
Quartz	$SiO_2 = +1.0\ SiO_2$	-3.9993
Dolomite	$CaMg(CO_3)_2 + 2H^+ = +1.0\,Ca^{++} + 1.0\ Mg^{++} + 2\ HCO_3^-$	2.5135
K-feldspar	$KAlSi3O8 + 4.0000\ H+ = + 1.0000\ Al+++ + 1.0000\ K+ + 2.0000\ H2O + 3.0000\ SiO2$	-0.2753
Brucite	$Mg(OH)_2 + 2H^+ = + 1.0\ Mg^{++} + 2H_2O$	16.2980
Tobermorite-11A	$Ca_5Si_6H_{11}O_{22.5} + 10H^+ = +5Ca^{++} + 6SiO_2 + 10.5H_2O$	65.6121
Saponite-Mg	$Mg3.165Al.33Si3.67O10(OH)2 + 7.3200\ H+ = + 0.3300\ Al+++ + 3.1650\ Mg++ + 3.6700\ SiO2 + 4.6600\ H2O$	26.2523
Nontronite-Mg	$Mg.165Fe2Al.33Si3.67H2O12 + 7.3200\ H+ = + 0.1650\ Mg++ + 0.3300\ Al+++ + 2.0000\ Fe+++ + 3.6700\ SiO2 + 4.6600\ H2O$	-11.6200
Talc	$Mg3Si4O10(OH)2 + 6.0000\ H+ = + 3.0000\ Mg++ + 4.0000\ H2O + 4.0000\ SiO2$	21.1383
Mesolite (Zeolite)	$Na.676Ca.657Al1.99Si3.01O10:2.647H2O + 7.9600\ H+ = + 0.6570\ Ca++ + 0.6760\ Na+ + 1.9900\ Al+++ + 3.0100\ SiO2 + 6.6270\ H2O$	13.6191
Stilbite (Zeolite)	$Ca1.019Na.136K.006Al2.18Si6.82O18:7.33H2O + 8.7200\ H+ = + 0.0060\ K+ + 0.1360\ Na+ + 1.0190\ Ca++ + 2.1800\ Al+++ + 6.8200\ SiO2 + 11.6900\ H2O$	1.0545

190

191   ### 3.2. Mineralogical analysis and kinetic information

192   The mineralogical composition of the BVG rock used in the experiment is shown in Table 3. The

193   concept of MKE was applied to the minerals existing in the rock that react with the ENFG leachate.

194   The initial mass of each reactant was calculated based upon its abundance in the 35 g BVG sample

195   (Rochelle et al. 2016; Rochelle et al. 1997). Note that the original rock sample showed some traces

196   of other fracture filling phases such as clays, but these were not included in the model.

197

198

199

Table 3: BVG rock sample composition. Analysis conducted by the British Geological Survey (Rochelle et al. 2016; Rochelle et al. 1997). The mass of each phase (m_0) is calculated based on a 35g rock sample.

Mineral	Weight %	m_0 (g)
Orthoclase	12	4.2
Quartz	41	14.35
Dolomite	29	10.15
Muscovite	13	4.55
Hematite	2	0.7
Calcite	3	1.05

When cement leachate encounters the surrounding host rock, they will be out of chemical equilibrium, and local dissolution of existing 'primary' minerals will occur. The process releases new solutes into the reaction system, resulting in the precipitation of new 'secondary' minerals. Some secondary phases can have enhanced sorption and permeability-limiting properties relative to the primary phases, and are thus beneficial in term of limiting radionuclide migration. Thus it is important to be able to describe/model the temporal evolution of these phases.

Commonly, the rate of mineral dissolution is measured experimentally by measuring the rate of change in solute concentration as a function of time under 'far from equilibrium' conditions. To model the experimental values of dissolution and precipitation, a variety of factors must first be addressed, which include: the reactive surface area of the mineral, initial and final amounts, the specific dissolution rate constant, and slowing of reaction as equilibrium is approached. The availability of these data is one of the challenges in the field of modelling mineral dissolution and precipitation. The MKE approach is implemented to overcome that drawback with a proper representation of the geochemical system. Equation 1 is a general form that is usually used to calculate the overall dissolution rate of minerals (Appelo and Postma 2005; Parkhurst and Appelo 1999; Rimstidt and Barnes 1980).

$$R_k = r_k \frac{A_0}{V} \left(\frac{m_k}{m_{0k}}\right)^n \quad (1)$$

222   where

$$r_k = k_k \left(1 - \left(\frac{IAP}{K}\right)_k\right) \quad (2)$$

224

225   R is the overall dissolution rate into solution (mol L^{-1} s^{-1}), k_k is the specific dissolution rate

226   (mol/m^2/s), A_0 is the initial surface area (m^2), V is the solution volume (L), m is the moles at a

227   given time and m_0 is the initial moles. $(m_k/m_{0k})^n$ is an interpretation of the changes in the reactive

228   surface area as a result of changes in the size of the mineral during the dissolution process. The

229   value of $n = 2/3$ (Appelo and Postma 2005). (IAP/K) (i.e., ion activity divided by equilibrium

230   constant) is equal to the saturation ratio *(SR)* of the reactant.

231

232   It is worth noting that clay minerals were not the focus of the original experiment, and that the

233   exact mica/clay phase(s) present in the fracture of the BVG rock were not fully identified (Moyce

234   et al. 2014). However, muscovite was chosen to represent this phase(s) in the modelling process

235   to control aluminium concentration in solution. Table 4 shows the kinetic information (reaction

236   rate constant, reactive surface area, solution volume) obtained from the literature for the minerals

237   in BVG that were modelled by the MKE approach (k-feldspar, quartz, dolomite, calcite,

238   muscovite). Conversely, hematite was modelled by the equilibrium approach only, because of its

239   low percentage in the rock sample (2%) and its assumed minimal influence on the mineralogical

240   evolution process. In terms of the precipitation process, for most minerals the kinetics and specific

241   rates of precipitation are unknown. Therefore, the precipitation of secondary phases was modelled

242   assuming control by thermodynamic equilibrium.

243 Table 4: Modelling parameters for the BVG rock. MKE (mixed kinetic equilibrium)

Mineral	Modelling	Solution Volume (L)	Surface area (m²/g)	Rate constant (mol m⁻² s⁻¹)
Orthoclase	MKE		0.02 (De Windt et al. 2008)	k (using equation 5) (Appelo and Postma 2005)
Quartz	MKE		0.02 (De Windt et al. 2008)	$k = 1x10^{-12.2}$ (70°C) (Worley 1994)
Dolomite	MKE		0.02 (De Windt et al. 2008)	$k= 1.2x10^{-12}$ (Appelo and Postma 2005) This value was lowered two orders of magnitude ($k= 1.2x10^{-10}$)
Muscovite	MKE	0.14 (Rochelle et al. 2016)	1.1 (Knauss 1989)	$k=10^{-18.1}$ (Knauss 1989)
Calcite	MKE		0.02 (De Windt et al. 2008)	$k1 = 10^{\wedge}(0.198 - 444.0 / (273.16 + T))$ $k2 = 10^{\wedge}(2.84 - 2177.0 / (273.16 + T))$ $k3 = 10^{\wedge}(-1.1 - 1737.0 / (273.16 + T))$ in which T denotes temperature. (Appelo and Postma 2005; Plummer et al. 1978)
Hematite	Equilibrium	-	-	-

244

245 *1) Quartz* (SiO_2)

246 As per equation (1) and (2), the overall dissolution kinetic equation for quartz will be:

247
$$R_{Quartz} = k_{Quartz}\left(\frac{A_0}{V}\right)\left(\frac{m}{m_0}\right)^{0.67}\left(1 - \left(\frac{IAP}{K}\right)_{Quartz}\right) \qquad (3)$$

248

249 *2) K-feldspar* ($KAlSi_3O_8$)
250

251 The overall dissolution rate proposed by (Appelo and Postma 2005; Parkhurst and Appelo 1999)

252 is used to simulate k-feldspar reaction at specific temperatures and pH value:

253
$$R_{K-feldspar} = k_{K-feldspar}\left(\frac{A_0}{V}\right)\left(\frac{m}{m_0}\right)^{0.67}\left(1 - \left(\frac{IAP}{K}\right)_{K-feldspar}\right) \qquad (4)$$

254 where

255
$$k_{K-feldspar} = k_{H^+}\frac{[H^+]^n}{f_H} + k_{H_2O}\frac{1}{f_{H_2O}} + k_{OH^-}\frac{[OH^-]^o}{f_{OH}} + k_{CO_2}\frac{[P_{CO_2}]^{0.6}}{f_{CO_2}} \qquad (5)$$

256

257   where $k_{K-feldspar}$ is the specific reaction rate (mol m^{-2} s^{-1}), k_i are the solute rate coefficients (mol

258   m^{-2} s^{-1}), and f_i are inhibition factors.

259

260   *3) Calcite $(CaCO_3)$*

261

262   The specific dissolution rate for calcite was described by (Appelo and Postma 2005; Parkhurst and

263   Appelo 1999; Plummer et al. 1978):

264

265
$$r_{calcite} = \left[k_1[H^+] + k_2[H_2CO_3] + k_3[H_2O]\right] * \left[1 - \left(\frac{IAP}{K}\right)^{\frac{2}{3}}_{Calcite}\right] \quad (6)$$

266
267   from equation (1), the overall dissolution rate of calcite will then be:
268

269
$$R_{calcite} = r_{calcite} \left(\frac{A_0}{V}\right)\left(\frac{m}{m_0}\right)^{0.67} \quad (7)$$

270
271   The value of the coefficients k_1, k_2 and k_3 in equations (6) are calculated by (Plummer et al. 1978)

272   by fitting them to the experimental data as a function of temperature.

273

274   *4) Dolomite $[CaMg(CO_3)_2]$*

275   The specific dissolution rate of dolomite is described below by (Appelo et al. 1984; Appelo and

276   Postma 2005; Parkhurst and Appelo 1999).

277
$$r_{Dolomite} = -k_{Dolomite} \, log\left(\frac{IAP}{K}\right)_{Dolomite} \quad (8)$$

278   then, the overall dissolution rate of dolomite will be:
279

280
$$R_{Dolomite} = r_{Dolomite} \left(\frac{A_0}{V}\right)\left(\frac{m}{m_0}\right)^{0.67} \quad (9)$$

281

282 *5) Muscovite $[KAl_2(AlSi_3O_{10})(OH)_2]$*

283

284 The specific dissolution rate for muscovite was calculated from the below equation, which was

285 described by (Knauss 1989):

286 $$r_{Muscovite} = 10^{-18.1}[a_{H^+}]^{+0.22} \quad (10)$$

287 then, as per equation (1), the overall dissolution rate of muscovite will be:

288

289 $$R_{Muscovite} = r_{Muscovite} \left(\frac{A_0}{V}\right) \left(\frac{m}{m_0}\right)^{0.67} \quad (11)$$

290

291   *3.3.Fluid evaporation*

292 Over the 15-year experiment period, (Rochelle et al. 2016; Rochelle et al. 1997) note that some of

293 the reacting fluid was lost, most likely through diffusion around the threads in the steel vessel.

294 Measures were not taken to limit this process, because the experiments were only initially planned

295 to only run for <18 months. The extent of this process could be estimated based on measured

296 increases in the concentration of conservative (i.e. inactive) dissolved ions in the experiment. In

297 both ENFG experiments (blank and reactive), the chloride ion was set as the inactive and

298 conservative species over the entire experiment period. It was observed that the rate of change in

299 chloride ion concentration was the same in both solutions, and amounted to a 34% fluid loss

300 (Moyce et al. 2014). It is crucial that modelling includes this fluid loss since this loss affects the

301 concentration value (usually measured in mg/L) of all the ions released into the solution. In the

302 modelling procedure, the simulated result of the chloride ion concentration indicated only a 22%
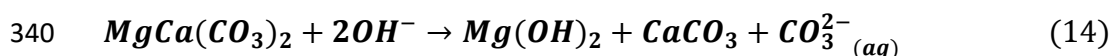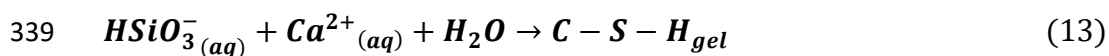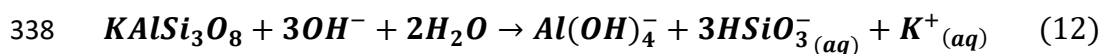
303 fluid loss.

304

305

306

307   *3.4.Secondary phases*

308   During the reaction period of 15 years, the chemical characteristics of the system would

309   significantly evolve and result in multiple cycles of mineral dissolution and precipitation reactions.

310   The type of precipitated secondary mineral can vary over the entire experimental period. In this

311   study, two time periods were defined: from 0 to 15 months (short-term mineral evolution) and

312   from 15 months to 15 years (long-term mineral evolution). In numerical simulations, the

313   specification of each expected secondary mineral was defined to allow its precipitation after

314   saturation. In the modelling process, attention was paid to minerals that were actually observed in

315   the experiments, together with ones that might precipitate (i.e. with saturation index close to zero),

316   in order to achieve more accurate results. Moreover, the list of secondary minerals being tracked

317   during the modelling should reasonably embrace the range of chemical ions represented in the

318   experiment. Finally, the stability range of realistic secondary phases being modelled should be

319   coincident with the experimental conditions (e.g. especially temperature and pH).

320

321   Several previous experimental studies have shown that when high-pH calcium-bearing cement

322   leachate reacts with the host rock in the CDZ, the primary silicate dissolves, followed mostly by

323   the precipitation of secondary CSH phases with different calcium-to-silicon ratios (Bateman et al.

324   1999; Braney et al. 1993; Gaucher and Blanc 2006; Hodgkinson and Hughes 1999; Mäder et al.

325   2006; Savage and Rochelle 1993). Where the system also includes aluminosilicate minerals

326   (Equations 12 and 13) and potassium (from minerals or the cement leachate), then secondary

327   phases of aluminium- and potassium-bearing minerals (C-[Al]-[K]-S-H) also precipitate (Braney

328   et al. 1993; Savage et al. 1992). Carbonate minerals, especially dolomite, can also play a significant

329   role in the precipitation of other, secondary carbonates (e.g., calcite, Equation 14) when reacting

330   with cement porewater leachate (Braithwaite and Heath 2013; Poole and Sotiropoulos 1980). Their

331   relatively fast dissolution reaction compared to silicate minerals can control fluid chemistry during

332   the early stages of the reaction (Bérubé et al. 1990; Choquette et al. 1991). Modelling studies have

333   also shown that the reaction time and the composition of the primary solution (e.g., pH) are the

334   two dominant factors in controlling the precipitating phases. Those studies also indicate that over

335   time, CSH gel will evolve into zeolite, feldspar and CSH minerals (Bateman et al. 1999; Braney

336   et al. 1993; Fernández et al. 2010; Pfingsten et al. 2006; Savage et al. 1992; Savage and Rochelle

337   1993; Soler and Mäder 2007).

338    $$KAlSi_3O_8 + 3OH^- + 2H_2O \rightarrow Al(OH)_4^- + 3HSiO_{3\ (aq)}^- + K^+_{(aq)} \qquad (12)$$

339    $$HSiO_{3\ (aq)}^- + Ca^{2+}_{\ (aq)} + H_2O \rightarrow C-S-H_{gel} \qquad\qquad (13)$$

340    $$MgCa(CO_3)_2 + 2OH^- \rightarrow Mg(OH)_2 + CaCO_3 + CO_{3\ (aq)}^{2-} \qquad\qquad (14)$$

341   As the BVG rock sample was rich in dolomite, it was assumed that the dedolomitization process

342   would result in an enormous number of magnesium and carbonate ions. This indicates that aqueous

343   calcium ions can also be a driving force for the dissolution process of dolomite, as well as the fluid

344   pH level. At the beginning of the experiments (from 0 to 15 months), there was a low concentration

345   of calcium ions in the YNFP, which led to undersaturation with respect to calcite and its

346   dissolution. However, in the ENFG fluid, the system had a high concentration of calcium ions,

347   which consumed all the aqueous ions of carbonate (CO_3^{2-}) to form the secondary calcite. Since

348   the rock sample also included quartz and feldspar, the released magnesium ions were expected to

349   react with both aqueous calcium and silica to form a secondary (Ca)-Mg-(Al)-(K)-silicate and

350   ettringite (In case sulphate ions were in the solution), as demonstrated in the literature (Derkowski

351   et al. 2013; Galí et al. 2001; Garcia et al. 2020; Schwarzenbach et al. 2013; Techer et al. 2012;

352   Tinseau et al. 2006; Xie et al. 2013). Studies have also confirmed the formation of talc, smectite

353   (Mg-saponite), illite and brucite as secondary Mg-rich phases during the dedolomitization process

354   (Chen et al. 2018; Moyce et al. 2014; Rochelle et al. 2016). Figure 3 shows the conceptual model

355   for mineral evolution during the dissolution and precipitation cycle of BVG rock reaction with

356   ENFG fluid.

357
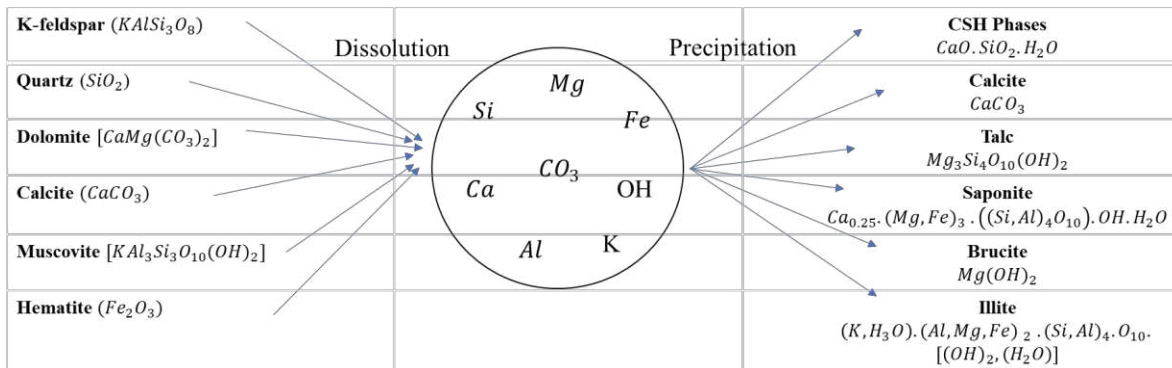
358

359 Figure 3: Conceptual model for minerals evolution during the dissolution and precipitation cycle of BVG reaction
360 with ENFG.

361

362 ### *4. Results and discussion*

363   The reaction of BVG rock with ENFG was modelled over a simulated 15-year duration using the

364   MKE approach. Changes in the concentration of Ca, Mg, Na, K, Al, Si, CO_3 and pH, as measured

365   from the experiment, were analysed in the modelling simulations, and the comparison is shown in

366   Figures 4–8. As an inactive ion, the chloride concentration (Figure 4, Plot A) increased in the

367   solution as a result of the evaporation process, in line with the experimental data. Furthermore,

368   since none of the primary minerals in the original rock sample included sodium and the potential

369   secondary phases did not significantly consume sodium, the increase in sodium concentration (Plot

370   A) also appears to be mainly a result of the evaporation process. This indicates that the sodium ion

371   is also a conservative species in this geochemical system.

372

373   The dissolution process of quartz, which accounts for 41% of the BVG rock, released a significant

374   amount of silicon into the highly alkaline solution in the first few months (Plot B). The availability

375   of silicon ions along with the initial calcium concentration (plus calcium released from the

376   dissolution of dolomite) then promoted the precipitation of secondary CSH and CASH phases,

377   represented by a sharp drop in silicon concentration along with a decrease in calcium concentration

378   (Plot C). The increase in potassium concentration (Plot D) was mostly linked to the evaporation

379   plus the dissolution of k-feldspar and muscovite, which also released silicon and aluminium. This

380   can be seen in the numerical results of Plot E, which show a small increase in aluminium

381   concentration in the first few months. The concentration line then drops heavily and follows the

382   experimental behaviour as a result of forming secondary aluminosilicate phases. The saturation

383   index lines in Figure 5 show that k-feldspar and muscovite both start with a higher dissolution rate

384   than quartz, which defines the small peak in aluminium concentration in the beginning before it

385   drops down as secondary calcium silicates start to precipitate. The figure also shows that muscovite

386   was always undersaturated, and thus would have continued to dissolve, providing a source of

387   aluminium for secondary phases. Moreover, the precipitation rates for talc, CSH gel and

388   tobermorite (CSH) were all high in the first few months of the reaction (Figure 7). This high

389   precipitation was mirrored by a substantial drop in silicon, aluminium and calcium concentrations

390   at almost the same time. Note that in Figure 7, the positive value is for the dissolving process,

391   whereas, negative for the precipitation process. Both CSH gel and tobermorite precipitated initially

392   and redissolved after 18 months, with a similar kinetic rate. Talc started to precipitate from the

393   beginning of the experiment and reached a stable amount after around 18 months. The initial

394   concentration of magnesium in the leachate, plus that released during dedolomitization, drove

395   brucite precipitation in the high pH conditions and created a sink for Mg (Bérubé et al. 1990;

396   Cheng 1986), which also consumed hydroxyl ions and reduced the pH value. This rapid drop in

397   pH in the first few months (Figure 4, Plot H) is also reflected in Figure 6, which shows a higher

398   precipitation rate of brucite in the same period. Subsequently, the drop in the pH value

399   progressively continued, but at a slower rate. From Figure 4 (Plot F), it is also clear that the initial

400   magnesium ions were consumed in the first few months before the dedolomitization process took

401   control. The saturation index of dolomite (Figure 5) shows that it was undersaturated (dissolving)

402   in the geochemical system, but with a much slower rate as the pH value went below 9. This agrees

403   with literature information (Min and Mingshu 1993), which suggests that dedolomitization does

404   not occur below pH 11. Despite that, dedolomitization still occurred in the geochemical system,

405   but at a very slow rate. This is demonstrated by the high magnesium concentration (Evaporation

406   can also play a part in this increase as well) at the end of the 15 years (Figure 4, Plot F), which was

407   observed in the experiment as well (Moyce et al. 2014). The escalation of dedolomitization can be

408   caused by the high concentration of Ca^{2+} in the ENFG, which promotes this process even at lower

409   pH values. Dedolomitization provides calcium and aqueous CO_3^{2-}, which are removed effectively

410   (Figure 4, Plot G) from the system by the precipitation of calcite (Bérubé et al. 1990). This can be

411   seen in the saturation indices of calcite and brucite (Figure 6), which both precipitate in

412   concurrence with the consumption of CO_3^{2-}. The extra amount of CO_3^{2-} in Equation 14 plus the

413   amount released from the dissolution of calcite at later stages of the experiment is also reflected in

414   Figure 4 (Plot G) which shows a small increase in (CO_3^{2-}) concentration. Thus, to incorporate the

415   slow dedolomitization process in the modelling, the specific dissolution rate of dolomite was

416   lowered by two orders of magnitude. This compensates for the slower dolomitisation process

417   below pH 11 but at the same time allows the process to take place, driven by the high concentration

418   of calcium ions, especially at the early stage of the reaction. Another indication that supports the

419 dedolomitization process is the high precipitation rate of Mg-silicate (talc and saponite-Mg), which

420 was reflected by the higher dissolution rate of dolomite in the same period. Since brucite was close

421 to saturation after the first few months (Figure 6), most of the released magnesium from the

422 dedolomitization process was likely consumed during the formation of magnesium-silicate

423 minerals, which is also recognised in other literature (Eglinton 1998; Glasser 2001).

424

425 After the large drop in the pH value, tobermorite and CSH gel starts to dissolve; at that time, a

426 substitution between aluminium and silicon ions takes place to produce more stable calcium

427 aluminosilicate hydrate (Myers et al. 2015; Richardson 2014; Richardson et al. 1993). This

428 secondary CASH phase can then bind with the magnesium from the dedolomitization and create

429 Mg-aluminosilicate (Galí et al. 2001; Moyce et al. 2014). This phenomenon highlights the

430 importance of the modelling procedure for this kind of complex long-term geochemical reaction,

431 as it allows a better understanding of the potential chemical and physical reactions that occur in

432 the geosphere. It can also allow the extension of the timescale from relatively short-duration lab

433 tests to the long timescales of performance assessments. Additionally, it can reveal the type of

434 dissolved or precipitated secondary minerals that can contribute effectively to the retardation of

435 radionuclide migration. For example, zeolites would be useful secondary phases as they have a

436 high sorption capability to the radionuclide. Their considerable surface area and ion exchange

437 capacity could play a key role in retarding radionuclide migration. Unfortunately, no evidence of

438 zeolite precipitation was found in any of the NSARP experiments (Moyce et al. 2014; Rochelle et

439 al. 2016). A plausible explanation for this is the rapid removal of silicon and aluminium by CSH

440 and CASH phases that could suppress the formation of zeolites as they may have slower kinetic

441 precipitation. Even though the modelling results obtained from the geochemical analysis showed

442 potential for mesolite, stilbite and scolecite precipitation (based on the temperature of the

443 experiment), which all are part of the zeolite family (Figure 8; (Bucher and Stober 2010; Bucher

444 and Weisenberger 2013; Fridriksson et al. 1999; Weisenberger and Selbekk 2009)).

445

446 Even though those minerals did not precipitate in the experiment, this does not prove that the

447 situation will be the same in the actual geosphere. The experimental design tried to mimic the

448 actual environmental conditions as much as possible (rock type, temp, pH, etc.). However, there

449 are still some variances, which can lead to different results. For example, as reported by (Adler et

450 al. 1999), zeolite formation is preferred in the pore spaces in which leachate flux is minimal, and

451 in these experiments the leachate: rock ratio was very high. The composition and nature of the

452 rock type can also play a significant role, as it can affect the amount of CO_2 released into the

453 leachate (e.g., depending on dolomite percentage), which can buffer the formation of zeolites

454 (Mullis et al. 1994; Weisenberger and Bucher 2010). Taken together, the findings reveal the

455 potentially important role of dolomite in the geochemical system. Moreover, they provide valuable

456 insight into specific geochemical processes alongside the usefulness of iterating between

457 modelling and experimental results to achieve a better understanding of the system under study.

458
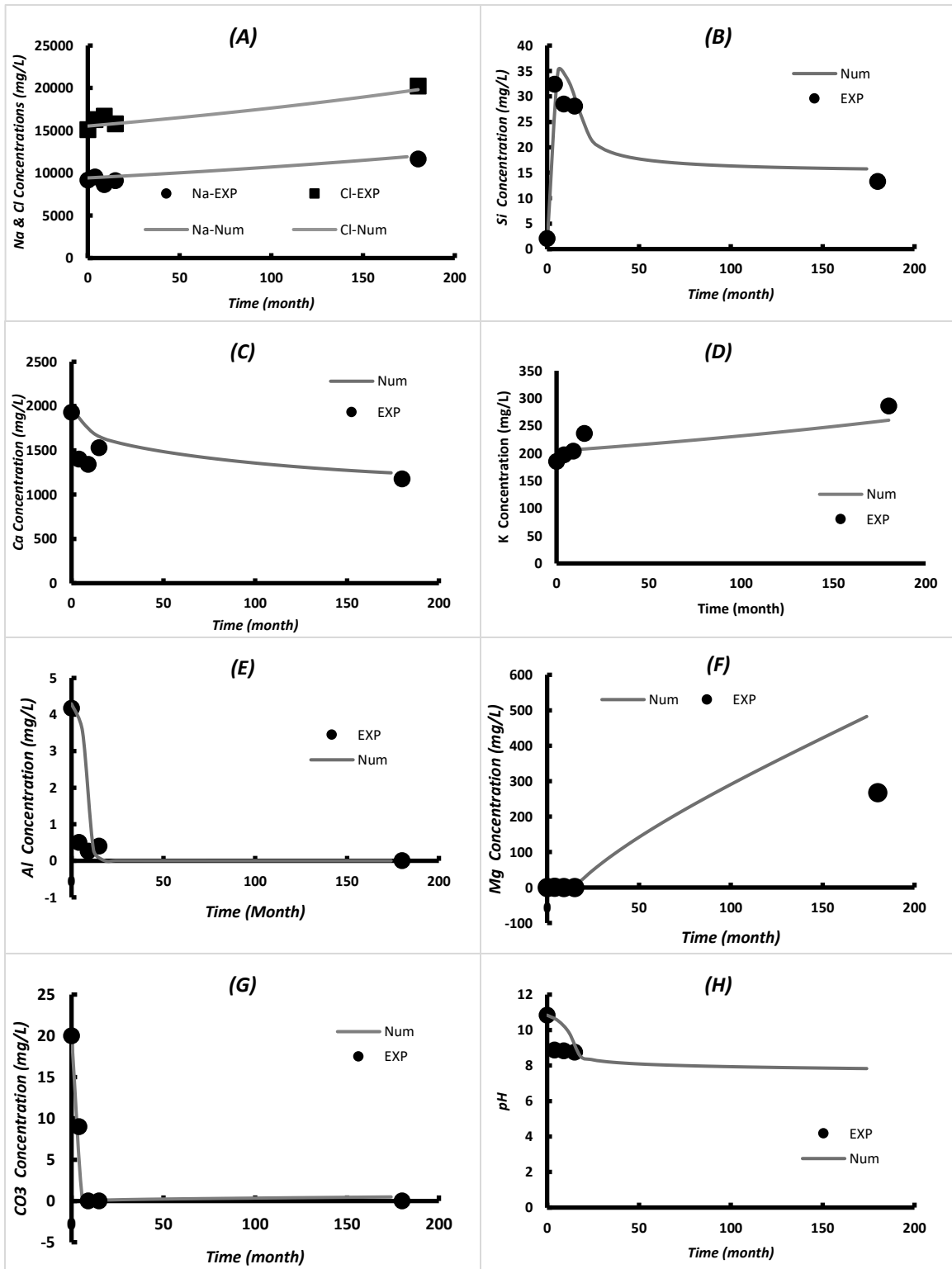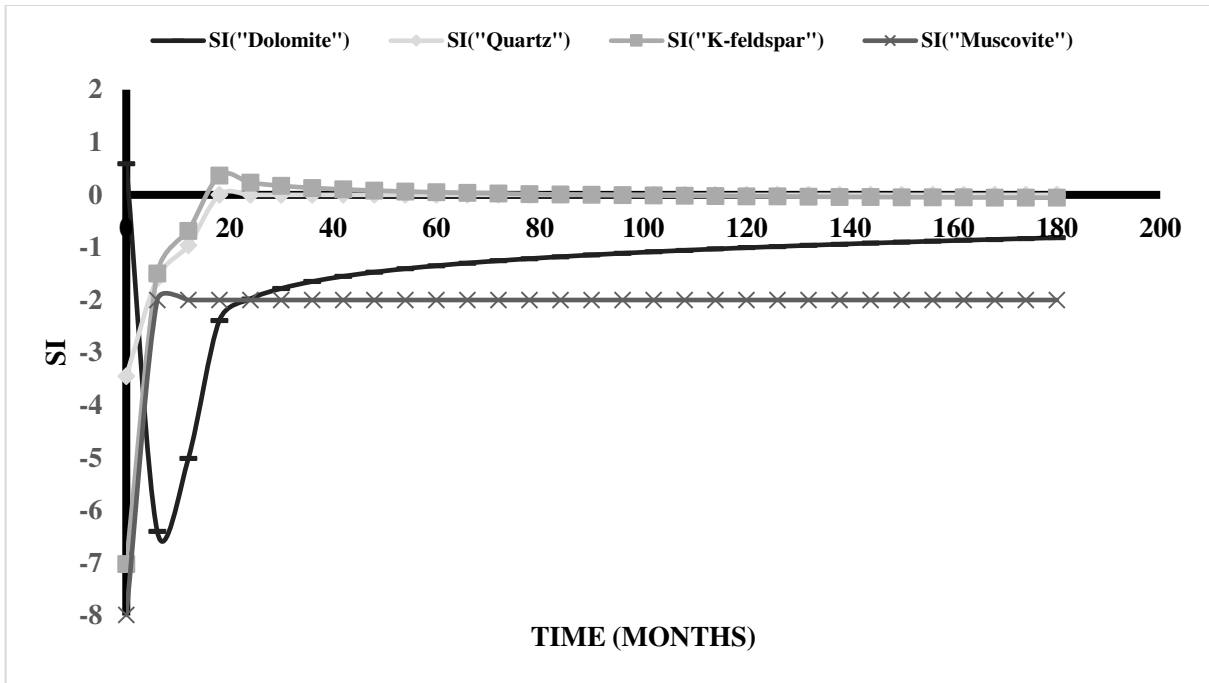
459

460

461

462

463

464

465

Figure 4: Modelled and experimental values for ions concentration and pH versus time.
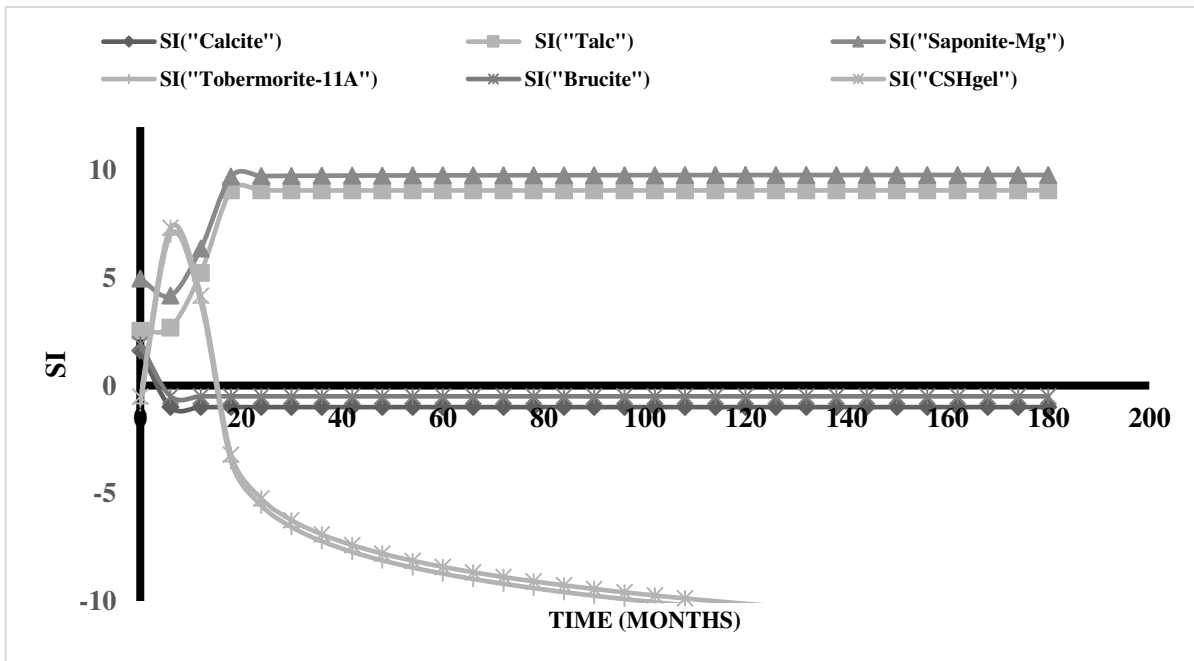
Figure 5: Saturation indices of primary mineral versus time.

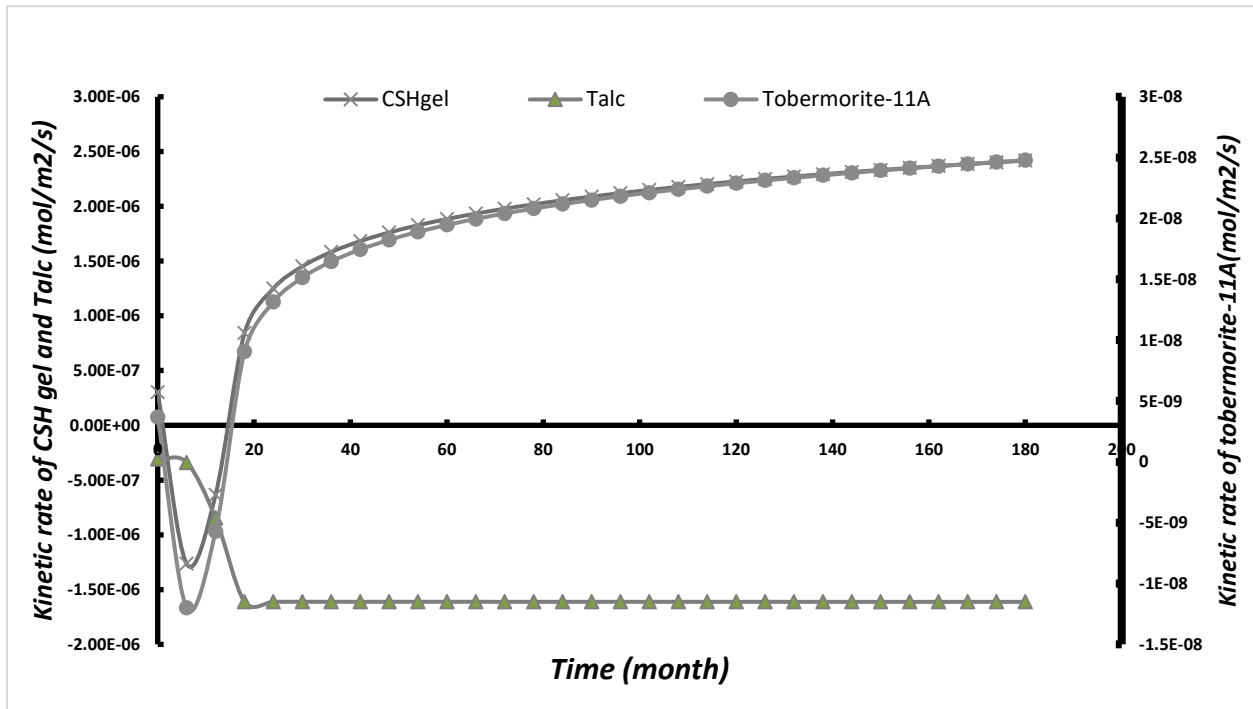Figure 6: Saturation indices of secondary phases versus time.
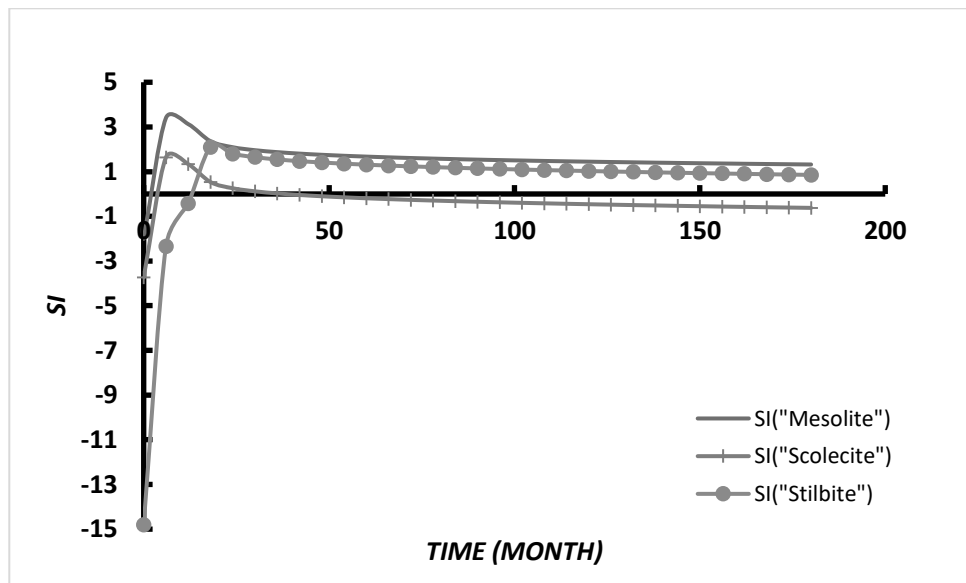
474

Figure 7: Kinetic rates for CSH gel, talc and tobermorite-11A versus time.

477

478

479

Figure 8: Zeolites minerals saturation indices versus time.

482

483   *5.   Conclusion*

484

485   The construction of a cement-based, deep underground geological disposal facility for radioactive

486   waste will result in an alkaline plume when groundwater equilibrates with minerals in the cement

487   barrier. This will initiate a series of dissolution/precipitation reactions in the surrounding host rock,

488   and consequent changes in physical, hydraulic, chemical and sorption properties long before any

489   potential migration of radionuclides. It is useful to understand and to be able to predict these

490   changes, as they are likely to influence the potential retardation of future radionuclide migration.

491   This study modelled the mineralogical evolution and geochemical reactions of BVG rock in

492   contact with ENFG. Importantly, the rock sample comprised a hydraulically-conductive dolomite-

493   rich fracture, and though dolomite is only a minor phase in the rock overall, it is a major phase in

494   direct contact with current groundwater. Simulations were conducted using PHREEQC, and

495   predictions compared with data from experiments lasting up to fifteen years. The results showed

496   that: (1) secondary phases such as talc, brucite and Mg-aluminosilicate precipitated, driven by

497   dedolomitization; (2) solution pH initially dropped quickly as a result of brucite precipitation; (3)

498   although zeolites were predicted stable secondary phases, they were absent in the experiments,

499   possibly as a consequence of factors such as slow reaction kinetics, high leachate-to-rock ratios or

500   elevated CO_2 concentrations. Overall, the modelling results of these long-term experiments

501   indicate the important role of fluid-mineral reactions in controlling fluid chemistry and secondary

502   phases, and so sufficient attention should be focused on the mineralogical composition of flowing

503   features, as the minerals lining those can exert a critical influence on key geochemical reactions.

504

505

512 ***References***

513

514 Adler M, Mäder U, Waber HN (1999) High-pH alteration of argillaceous rocks: an experimental study
515   Schweiz Mineral Petrogr Mitt 79:445-454
516 Appelo C, Beekman H, Oosterbaan AJIP (1984) Hydrochemistry of springs from dolomite reefs in the
517   southern Alps of northern Italy 150:125-138
518 Appelo C, Postma DJB, Roterdam (2005) Geochemistry, groundwater and pollution, CRC
519 Atkinson A, Everitt N, Guppy R (1988) Evolution of pH in a radwaste repository: Internal reactions
520   between concrete constituents. UKAEA Harwell Lab.(UK). Materials Development Div,
521 Authority ND (2010a) Geological Disposal: Near-field evolution status report. NDA Report
522   NDA/RWMD/033,
523 Authority ND (2010b) Geological Disposal: Steps Towards Implementation Nuclear Decommissioning
524   Authority Report NDA/RWMD/013
525 Bateman K, Coombs P, Noy D, Pearce J, Wetton P, Haworth A, Linklater C (1999) Experimental
526   simulation of the alkaline disturbed zone around a cementitious radioactive waste repository:
527   numerical modelling and column experiments Geological Society, London, Special Publications
528   157:183-194
529 Berner U (1990) A thermodynamic description of the evolution of pore water chemistry and uranium
530   speciation during the degradation of cement. Paul Scherrer Inst.(PSI),
531 Bérubé M-A, Choquette M, Locat J (1990) Effects of lime on common soil and rock forming minerals
532   Applied Clay Science 5:145-163
533 Bethke C (1994) The Geochemist's Workbench, Version 2.0: A Users Guide to Rxn, Act2, Tact, React,
534   and Gtplot. Craig M. Bethke,
535 Bethke C (1996) Geochemical reaction modeling: Concepts and applications. Oxford University Press on
536   Demand,
537 Blanc P, Lassin A, Piantone P, Azaroual M, Jacquemet N, Fabbri A, Gaucher EC (2012) Thermoddem: A
538   geochemical database focused on low temperature water/rock interactions and waste materials
539   Applied Geochemistry 27:2107-2116
540 Braithwaite CJ, Heath RA Alkali–carbonate reactions and 'dedolomitization'in concrete: silica, the
541   elephant in the corner. In, 2013. Geological Society of London,
542 Braney MC, Haworth A, Jefferies NL, Smith AC (1993) A study of the effects of an alkaline plume from
543   a cementitious repository on geological materials Journal of Contaminant Hydrology 13:379-402
544   doi:https://doi.org/10.1016/0169-7722(93)90072-Z
545 Brun A, Engesgaard P (2002) Modelling of transport and biogeochemical processes in pollution plumes:
546   literature review and model development Journal of Hydrology 256:211-227
547   doi:https://doi.org/10.1016/S0022-1694(01)00547-9
548 Bucher K, Stober I (2010) Fluids in the upper continental crust Geofluids 10:241-253

Bucher K, Weisenberger TB (2013) Fluid-induced mineral composition adjustments during exhumation: the case of Alpine stilbite Contributions to Mineraluogy and Petrology 166:1489-1503

Chen X, Pao W, Thornton S, Small J (2016) Unsaturated hydro-mechanical–chemical constitutive coupled model based on mixture coupling theory: Hydration swelling and chemical osmosis International Journal of Engineering Science 104:97-109

Chen X, Thornton S (2018) Multi-Mineral Reactions Controlling Secondary Phase Evolution in a Hyper-Alkaline Plume Environmental Geotechnics

Chen X, Thornton SF, Pao WJIJoES (2018) Mathematical model of coupled dual chemical osmosis based on mixture-coupling theory 129:145-155

Chen X, Thornton SF, Small J (2015) Influence of hyper-alkaline pH leachate on mineral and porosity evolution in the chemically disturbed zone developed in the near-field host rock for a nuclear waste repository Transport in Porous Media 107:489-505

Cheng K Chemical consumption during alkaline flooding: A comparative evaluation. In: SPE Enhanced Oil Recovery Symposium, 1986. Society of Petroleum Engineers,

Choquette M, Berube M-A, Locat J (1991) Behavior of common rock-forming minerals in a strongly basic NaOH solution The Canadian Mineralogist 29:163-173

De Windt L, Marsal F, Tinseau E, Pellegrini DJP, Chemistry of the Earth PABC (2008) Reactive transport modeling of geochemical interactions at a concrete/argillite interface, Tournemire site (France) 33:S295-S305

Delany J, Lundeen S (1990) The LLNL thermochemical database Lawrence Livermore National Laboratory Report UCRL-21658 150

Derkowski A, Bristow TF, Wampler JM, Środoń J, Marynowski L, Elliott WC, Chamberlain CP (2013) Hydrothermal alteration of the Ediacaran Doushantuo Formation in the Yangtze Gorges area (South China) Geochimica et Cosmochimica Acta 107:279-298 doi:https://doi.org/10.1016/j.gca.2013.01.015

Eglinton M (1998) Resistance of concrete to destructive agencies Lea's chemistry of cement and concrete

Fernández R, Rodríguez M, Villa RVdl, Cuevas J (2010) Geochemical constraints on the stability of zeolites and C–S–H in the high pH reaction of bentonite Geochimica et Cosmochimica Acta 74:890-906 doi:https://doi.org/10.1016/j.gca.2009.10.042

Francis A, Cather R, Crossland IJNSRS, United Kingdon Nirex Limited, 57p (1997) Development of the Nirex Reference Vault Backfill; report on current status in 1994

Fridriksson T, Neuhoff P, Bird D, Arnórsson S (1999) Clays and zeolites record alteration history at Teigarhorn, eastern Iceland Geochemistry of the earth's surface Balkema, Rotterdam:377-380

Galí S, Ayora C, Alfonso P, Tauler E, Labrador M (2001) Kinetics of dolomite–portlandite reaction: Application to portland cement concrete Cement and Concrete Research 31:933-939 doi:https://doi.org/10.1016/S0008-8846(01)00499-9

Garcia E, Alfonso P, Tauler E (2020) Mineralogical Characterization of Dolomitic Aggregate Concrete: The Camarasa Dam (Catalonia, Spain) Minerals 10:117

Gaucher EC, Blanc P (2006) Cement/clay interactions – A review: Experiments, natural analogues, and modeling Waste Management 26:776-788 doi:https://doi.org/10.1016/j.wasman.2006.01.027

Glasser FP (2001) Mineralogical aspects of cement in radioactive waste disposal Mineralogical Magazine 65:621-633

Harris A, Hearne J, Nickerson A (2001a) The effect of reactive groundwaters on the behaviour of cementitious materials. AEA Technology Report AEAT/R/ENV/0467,

Harris A, Manning M, Thompson A (2001b) Testing of models of the dissolution of cements-leaching behaviour of Nirex Reference Vault Backfill. In: AEA Technology Report, AEAT/ERRA-0316. Nirex Ltd. Harwell, UK,

Hoch A, Baston G, Glasser F, Hunter F, Smith V (2012) Modelling evolution in the near field of a cementitious repository Mineralogical Magazine 76:3055-3069

598   Hodgkinson ES, Hughes CR (1999) The mineralogy and geochemistry of cement/rock reactions: high-
599   resolution studies of experimental and analogue materials Geological Society, London, Special
600   Publications 157:195-211
601   Kim Y-K et al. (2007) The Korean Final Repository for Low- and Intermediate-Level Radioactive
602   Waste:1383-1387 doi:10.1115/ICEM2007-7130
603   Knauss KGJGeCA (1989) Muscovite dissolution kinetics as a function of pH and time at 70 C 53:1493-
604   1501
605   Lichtner PC (1996) Continuum formulation of multicomponent-multiphase reactive transport Reviews in
606   mineralogy 34:1-82
607   Lothenbach B et al. (2019) Cemdata18: A chemical thermodynamic database for hydrated Portland
608   cements and alkali-activated materials Cement and Concrete Research 115:472-506
609   Mäder UK et al. (2006) Interaction of hyperalkaline fluid with fractured rock: Field and laboratory
610   experiments of the HPF project (Grimsel Test Site, Switzerland) Journal of Geochemical
611   Exploration 90:68-94 doi:https://doi.org/10.1016/j.gexplo.2005.09.006
612   Mayer KU, Frind EO, Blowes DW (2002) Multicomponent reactive transport modeling in variably
613   saturated porous media using a generalized formulation for kinetically controlled reactions Water
614   Resources Research 38:13-11-13-21
615   Min D, Mingshu T (1993) Mechanism of dedolomitization and expansion of dolomitic rocks Cement and
616   Concrete Research 23:1397-1408
617   Moyce EB et al. (2014) Rock alteration in alkaline cement waters over 15 years and its relevance to the
618   geological disposal of nuclear waste 50:91-105
619   Mullis J, Dubessy J, Poty B, O'Neil J (1994) Fluid regimes during late stages of a continental collision:
620   Physical, chemical, and stable isotope measurements of fluid inclusions in fissure quartz from a
621   geotraverse through the Central Alps, Switzerland Geochimica et cosmochimica Acta 58:2239-
622   2267
623   Myers RJ, L'Hôpital E, Provis JL, Lothenbach B (2015) Effect of temperature and aluminium on calcium
624   (alumino) silicate hydrate chemistry under equilibrium conditions Cement and Concrete Research
625   68:83-93
626   Parkhurst DL, Appelo C (1999) User's guide to PHREEQC (Version 2): A computer program for
627   speciation, batch-reaction, one-dimensional transport, and inverse geochemical calculations
628   Pfingsten W, Paris B, Soler JM, Mäder UK (2006) Tracer and reactive transport modelling of the
629   interaction between high-pH fluid and fractured rock: Field and laboratory experiments Journal of
630   Geochemical Exploration 90:95-113
631   Plummer L, Wigley T, Parkhurst DJAjos (1978) The kinetics of calcite dissolution in CO 2-water systems
632   at 5 degrees to 60 degrees C and 0.0 to 1.0 atm CO 2 278:179-216
633   Poole A, Sotiropoulos P (1980) Reactions between dolomitic aggregate and alkali pore fluids in concrete
634   Quarterly Journal of Engineering Geology and Hydrogeology 13:281-287
635   Prommer H, Barry D, Zheng C (2003) MODFLOW/MT3DMS-based reactive multicomponent transport
636   modeling Groundwater 41:247-257
637   Richardson IG (2014) Model structures for c-(a)-sh (i) Acta Crystallographica Section B: Structural
638   Science, Crystal Engineering and Materials 70:903-923
639   Richardson IG, Brough AR, Brydson R, Groves GW, Dobson CM (1993) Location of aluminum in
640   substituted calcium silicate hydrate (C-S-H) gels as determined by 29Si and 27Al NMR and
641   EELS Journal of the American Ceramic Society 76:2285-2288
642   Rimstidt JD, Barnes HJGeCA (1980) The kinetics of silica-water reactions 44:1683-1699
643   Rochelle C, Milodowski A, Bateman K, Moyce E, Hudson-Edwards K (2016) A long-term experimental
644   study of the reactivity of basement rock with highly alkaline cement waters: Reactions over the
645   first 15 months Mineralogical Magazine 80:1089-1113
646   Rochelle C, Pearce J, Bateman K, Coombs P, Wetton P (1997) The Evaluation of Chemical Mass
647   Transfer in the Disturbed Zone of a Deep Geological Disposal Facility for Radioactive Wastes. X,
648   Interaction Between Synthetic Cement Porefluids and BVG: observations from Experiments of 4,

649   9, and 15 Months Duration: British Geological Survey, Fluid Processes Series, Technical Report
650   WE/97/016.
651 Savage D et al. (1992) Rate and mechanism of the reaction of silicates with cement pore fluids Applied
652   Clay Science 7:33-45
653 Savage D, Rochelle CA (1993) Modelling reactions between cement pore fluids and rock: implications
654   for porosity change Journal of Contaminant Hydrology 13:365-378
655   doi:https://doi.org/10.1016/0169-7722(93)90071-Y
656 Schwarzenbach EM, Lang SQ, Früh-Green GL, Lilley MD, Bernasconi SM, Méhay S (2013) Sources and
657   cycling of carbon in continental, serpentinite-hosted alkaline springs in the Voltri Massif, Italy
658   Lithos 177:226-244 doi:https://doi.org/10.1016/j.lithos.2013.07.009
659 Schwyn B, Wersin P, Berner U, Wieland E, Neall F (2003) Near-field chemistry of an ILW repository in
660   Opalinus Clay Unpubl Nagra Internal Rep Nagra, Wettingen, Switzerland
661 Skogsberg M, Ingvarsson R (2006) Operational experience from SFR-Final repository for low-and
662   intermediate level waste in Sweden.
663 Small J, Bryan N, Lloyd J, Milodowski A, Shaw S, Morris K (2016) Summary of the BIGRAD project
664   and its implications for a geological disposal facility National Nuclear Laboratory, Report NNL
665   (16) 13817
666 Soetaert K, Herman PM, Middelburg JJJGeCA (1996) A model of early diagenetic processes from the
667   shelf to abyssal depths 60:1019-1040
668 Soler JM, Mäder UK (2007) Mineralogical alteration and associated permeability changes induced by a
669   high-pH plume: Modeling of a granite core infiltration experiment Applied Geochemistry 22:17-
670   29 doi:https://doi.org/10.1016/j.apgeochem.2006.07.015
671 Techer I, Bartier D, Boulvais P, Tinseau E, Suchorski K, Cabrera J, Dauzères A (2012) Tracing
672   interactions between natural argillites and hyper-alkaline fluids from engineered cement paste and
673   concrete: Chemical and isotopic monitoring of a 15-years old deep-disposal analogue Applied
674   Geochemistry 27:1384-1402 doi:https://doi.org/10.1016/j.apgeochem.2011.08.013
675 Tinseau E, Bartier D, Hassouta L, Devol-Brown I, Stammose D (2006) Mineralogical characterization of
676   the Tournemire argillite after in situ interaction with concretes Waste Management 26:789-800
677   doi:https://doi.org/10.1016/j.wasman.2006.01.024
678 Van der Lee J (1997) HYTEC, un modèle couplé hydro-géochimique de migration de polluants et de
679   colloïdes. In: Technical Report LHM/RD/97/02. CIG, École des Mines de Paris Fontainbleau,
680   France,
681 Van der Lee J (1998) Thermodynamic and mathematical concepts of CHESS
682 Weisenberger T, Bucher K (2010) Zeolites in fissures of granites and gneisses of the Central Alps Journal
683   of Metamorphic Geology 28:825-847
684 Weisenberger T, Selbekk RS (2009) Multi-stage zeolite facies mineralization in the Hvalfjördur area,
685   Iceland International Journal of Earth Sciences 98:985-999
686 Westall J (1986) „Zachary, J. L „Morel, FMM: MINEQL, a computer program for the calculation of the
687   chemical equilibrium composition of aqueous systems. Tech. Note,
688 Wolery TJ (1992) EQ3/6, a software package for geochemical modeling of aqueous systems: package
689   overview and installation guide (version 7.0)
690 Wolery TJ, Daveler SA (1992) EQ6, a computer program for reaction path modeling of aqueous
691   geochemical systems: Theoretical manual, users guide, and related documentation (Version 7.0);
692   Part 4. Lawrence Livermore National Lab., CA (United States),
693 Worley WG (1994) Dissolution kinetics and mechanisms in quartz-and grainite-water systems.
694   Massachusetts Institute of Technology
695 Xie Q et al. (2013) Mechanism of palygorskite formation in the Red Clay Formation on the Chinese
696   Loess Plateau, northwest China Geoderma 192:39-49
697   doi:https://doi.org/10.1016/j.geoderma.2012.07.021

698